Journal of Power Sources 189 (2009) 211–216

Contents lists available at ScienceDirect

Journal of Power Sources

journal homepage: www.elsevier.com/locate/jpowsour

Li–B–O–N electrolytes for all-solid-state thin film batteries

J.M. Kim [a], G.B. Park [a], K.C. Lee [a], H.Y. Park [a,*], S.C. Nam [a], S.W. Song [b]

[a] Microcell Center, Nuricell Inc., Seoul 134-848, Republic of Korea
[b] Department of Fine Chemical Engineering & Applied Chemistry, Chungnam National University, Daejeon 305-764, Republic of Korea

ARTICLE INFO

Article history:
Received 25 June 2008
Received in revised form
20 September 2008
Accepted 22 September 2008
Available online 2 October 2008

Keywords:
Li–B–O–N
Electrolyte
All-solid-state
Thin film battery

ABSTRACT

We report for the first time new Li^+ ion conducting thin film solid electrolytes based on Li–B–O–N system. Substitution of oxygen in xLi_2O–B_2O_3 (x = 1, 3, 5) by nitrogen was successfully achieved by reactive sputtering under nitrogen plasma. FTIR and XPS analyses indicated that N atom was incorporated in the Li–B–O matrix film, and an increase in the composition of Li_2O together with N-substitution caused the structural conversion from ring-type borate to open structured one, where more free space and ionic bonding characteristic are offered for higher mobility of Li^+ ions. A high ionic conductivity of ca. 2.3×10^{-6} S cm^{-1} at room temperature was obtained from the thin film electrolyte of $Li_{3.09}BO_{2.53}N_{0.52}$ glass that was prepared using $3Li_2O$–B_2O_3 target. Electrochemical analyses suggest the high Li^+ ion conductivity is induced by the reduced activation energy through the control of the composition and the structure.

1. Introduction

It has been widely understood that all-solid-state power sources are promising for improving safety and reliability of electronic devices. Fast Li^+ ion conducting solid electrolytes are appealing due to their potential application in all-solid-state batteries and other solid-state electrochemical devices (e.g. sensors, electrochromic devices). Present Li-ion batteries based on liquid organic electrolyte have disadvantages; the formation of a solid electrolyte interface (SEI) at the anode leads to a large irreversible capacity loss during cycling, and there are safety and self-discharge concerns. In this respect, the development of alternative solid electrolytes is a critical issue for advanced lithium batteries.

High priority criteria of solid electrolyte to achieve high energy density and long-term stability are high Li^+ ion conductivity, low electronic conductivity, stability against chemical reaction with electrodes and wide stability window (high decomposition voltage). There are several candidates of solid electrolytes based on oxides and non-oxides (e.g. halides, sulfides, nitrides) system classified by their elements and by crystallinity. Some solid electrolytes composed of non-oxide system showed several failure modes of unstability in ambient condition as well as in the potential range on normal Li battery operation or the corrosion of vacuum chamber, despite reasonable ionic conductivity (~10^{-3} to 10^{-5} S cm^{-1}). Compared to crystalline electrolyte that has a narrow composition range and an anisotropic conductivity, glassy oxide system seems to be appropriate for inorganic solid electrolyte with reduced internal resistance, despite the relatively small conductivity (~10^{-6} S cm^{-1}).

Relevant reports of excellent glass-ceramic thin film electrolytes for thin film battery is rare, except lithium phosphorous oxynitride (Lipon) [1,2]. Lipon films typically deposited by RF sputtering using Li_3PO_4 target in nitrogen plasma is known to be effectively stabilized in contact with metallic lithium and enhance its ionic mobility due to either the formation of additional phosphate cross-linking or reduced electrostatic energy. Maximum ionic conductivity at room temperature reported is ca. 2×10^{-6} S cm^{-1} for $Li_{2.9}PO_{3.3}N_{0.46}$. Although Lipon functions excellently in Li thin film batteries, changes in oxidation state of P atom as −3, +1 and +5 during cycling can possibly cause the variation in electronic conductivity [3,4]. Several research groups reported [5,6] no significant change in composition between the films and the starting materials in xLi_2O–B_2O_3 thin film systems, and low ionic conductivity of $0.5–1.0 \times 10^{-7}$ S cm^{-1} at room temperature for the $3Li_2O$–B_2O_3 film. It is generally recognized that transferring the composition of source materials to film with vacuum evaporation technique is difficult to achieve.

Recently we successfully prepared Li–B–O–N thin film electrolytes. We report here for the first time the nitrogen substitution for oxygen in borate group of xLi_2O–B_2O_3 (x = 1, 3, 5) and its effect on structure and ionic conductivity. Although oxynitride glasses are known to difficult to prepare by conventional process starting from alkali borate glasses [7], we achieved the incorporation of nitrogen

* Corresponding author. Tel.: +82 2 6900 4154; fax: +82 2 6900 4160.
E-mail addresses: hypark@nuricell.com, hypark@korea.ac.kr (H.Y. Park).

0378-7753/$ – see front matter © 2008 Elsevier B.V. All rights reserved.
doi:10.1016/j.jpowsour.2008.09.089

into lithium borate glass thin film by non-equilibrium reaction by sputtering method. The Li–B–O–N thin film electrolytes showed a significantly improved ionic conductivity and enhanced chemical stability. The electrochemical properties could be manipulated by the modification of borate structures by altering Li composition and N-doping level.

2. Experimental

A 13.56 MHz RF magnetron sputtering system with a sputter down geometry was used to deposit the Li–B–O–N glassy electrolyte films. Sintered sputtering targets in 4-in. diameter (ULVAC Materials, Inc.) were prepared with compositions of Li_2O–B_2O_3 (1LBO), $3Li_2O$–B_2O_3 (3LBO) and $5Li_2O$–B_2O_3 (5LBO). Films sputtered on 18 mm × 24 mm × 0.25 mm alumina substrates (CoorsTek) using each targets with variable composition are called as 1Li–B–O–N, 3Li–B–O–N and 5Li–B–O–N henceforth, respectively. The substrates were covered by metal masks with various shapes patterned for each layer of thin film battery components. Solid electrolyte properties of ion conductivity and stable potential window were measured using blocking electrodes cells stacked in the form of Pt/Li–B–O–N/Pt. Complete thin film batteries were fabricated by depositing Pt (250 nm)/$LiCoO_2$ (1.5 μm)/Li–B–O–N (1.5 μm) sequentially, using DC/RF sputtering, and Li (1.0 μm) film was finally deposited on Li–B–O–N by thermal evaporation. The $LiCoO_2$ cathode layer was annealed by rapid thermal annealing (RTA) at 600 °C before electrolyte sputtering as described elsewhere [8].

The thickness of films was measured using a surface profiler (Alpha step 500, Tenco). Surface morphologies and cross-section of films were observed by field emission scanning electron microscopy (FESEM, Inspect F, FEI). The film composition was determined from elastic recoil detection-time of flight (ERD-TOF). The crystal structure of Li–B–O–N was examined by X-ray diffraction spectrometer (XRD, RINT/DMAS-2500, Rigaku). Structure of the Li–B–O–N films was examined by FTIR spectroscopy, using IR spectrometer (Bruker optics IFS66V/S) equipped with a MCT detector. The FTIR spectra were acquired in the ATR mode using a Ge optic. Spectral resolution was of 4 cm^{-1} and total of 512 scans were co-added. For identifying N-doping, XPS measurement was conducted using a focused monochromatic Al Kα source for excitation and a spherical section analyzer (Axis-Nova, Kratos). The pass energy was 20 eV, giving an overall energy resolution of 0.05 eV. The spectra were recorded under a pressure of 5.0×10^{-9} Torr, and the irradiated spot size was 200 μm. The binding energy was calibrated based on C 1s level at 284.6–284.8 eV.

Electrochemical impedance spectroscopy (EIS) was performed for measuring ionic conductivity at room temperature using blocking electrodes cells in the AC frequency range of 1 MHz to 50 mHz using EIS analyzer (IM6ex, Zhaner). The potential window stability at 0–5 V was examined by linear sweep voltammetry (LSV) at a scan rate of 0.5 mV s^{-1} at room temperature. Charge–discharge behavior of a full thin film battery was tested by constant current cycling at 0.075 mA cm^{-2}.

3. Results and discussion

3.1. Physical analyses of Li–B–O–N thin films

All as-deposited Li–B–O–N thin films were amorphous, determined by X-ray diffraction analyses (Fig. 1), suggesting that the Li–B–O–N is glassy materials. The surface morphologies obtained by FESEM exhibit a smooth and dense film without grain boundaries, indicating that our reactive sputtering was useful to form glassy ceramic thin films (Fig. 2). Table 1 shows the elemental analyses data obtained from ERD-TOF analyses. The film compositions were similar to those of target materials, except that lithium to boron (Li:B) ratio of 3.5:1 is smaller than the theoretical value 5:1 of 5Li–B–O–N. As increasing lithium content, the amount of nitrogen incorporated in the film decreased.

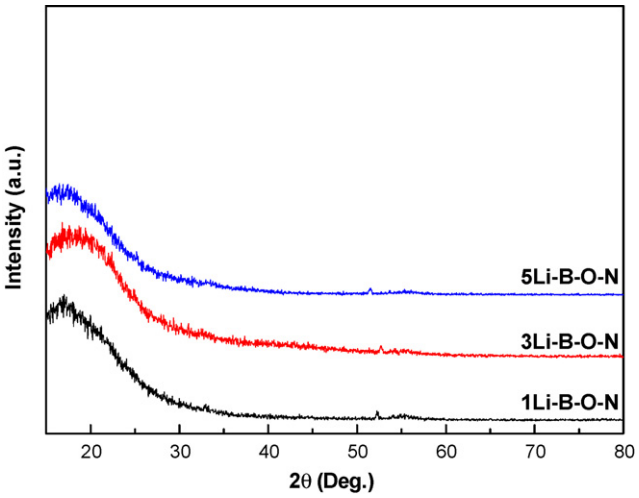

Fig. 1. X-ray diffraction patterns of the 1, 3 and 5Li–B–O–N thin films.

Structural changes from LBO target to N-doped film were characterized using ATR FTIR spectroscopy. Fig. 3 compares the FTIR spectra of the 3LBO target with 3Li–B–O–N film. The LBO target shows a dominant peak at 1411 cm^{-1}, attributed to stretching mode of B-O of BO_3 unit in six-membered boroxol ring [5,9,10]. A peak at 1146 cm^{-1} and a shoulder near 1250 cm^{-1} are attributable to B–O stretching modes of BO_4 unit from pyroborate and tetraborate, respectively, which is not observable for B_2O_3 with only boroxol ring structure [5,9,10]. Other fingerprints in the low frequency region confirm this assignment. By the addition of Li_2O, some boroxol ring seems to be destroyed to open-type structure and non-bridging oxygen appears to be created. For N-doped film, the peak due to boroxol ring is absent, but the shoulder peak intensity at 1254 cm^{-1}, attributable to stretching modes of B–O/B–N, is remarkably enhanced. This indicates that N-doping contributes to destroy the boroxol ring structure to meta-/tri-/tetra-borate type structures. Significant intensity enhancement of the peak at 760 cm^{-1}, attributed to deformation modes of B–O–B/B–N–B bonds, reflects that more amounted open-type B–O(N)–B bondings were produced at the expense of boroxol ring-type bonding.

Such structural changes were more significant for the films with higher lithium content as shown in Fig. 4. As increasing lithium content, the peak at 1145 cm^{-1} due to BO_4 of pyroborate remained almost unchanged, but the shoulder peak near 1300 cm^{-1}, attributed to stretching modes of B–O/B–N, shifted downward. This red shift is associated with local structural change from meta-/tri-/tetra-borate, which posses some ring structure and BO_4 units, to pyroborate type structure that has only repeated BO_3

Table 1
Elemental analyses results for Li–B–O–N thin films.

Elements	1Li–B–O–N	3Li–B–O–N	5Li–B–O–N
Li	0.903	3.099	3.506
B	1.000	1.000	1.000
O	0.658	2.532	3.030
N	0.984	0.516	0.515
Composition (Li:B:O:N)	0.90:1.00:0.66:0.98	3.09:1.00:2.53:0.52	3.51:1.00:3.03:0.52

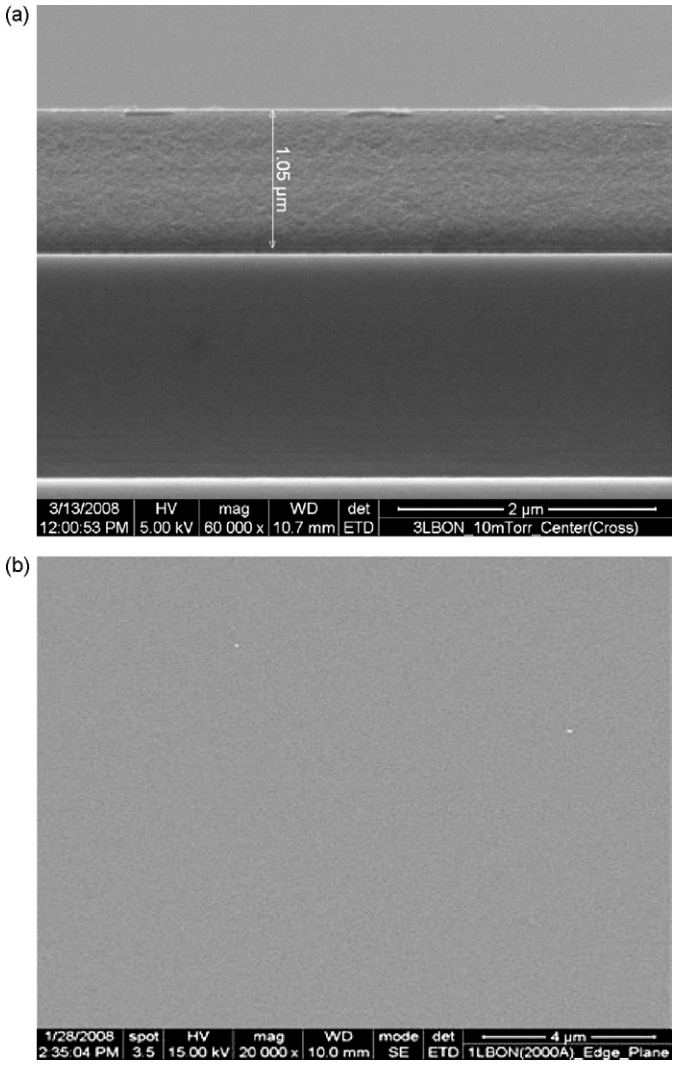

Fig. 2. SEM images for (a) cross-section of 3Li–B–O–N film and (b) surface of 1Li–B–O–N film.

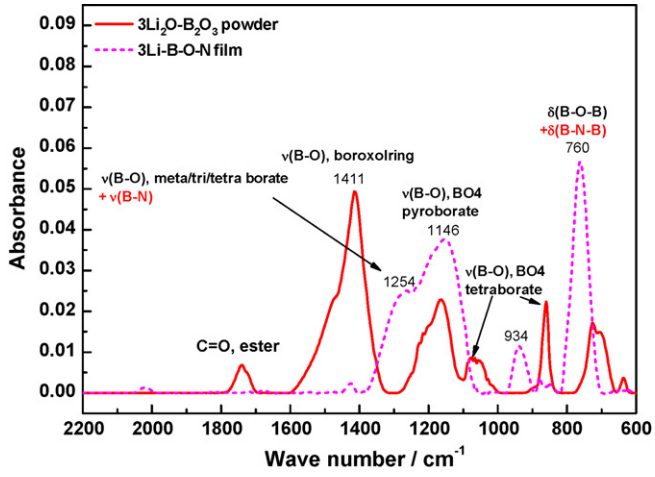

Fig. 3. FTIR spectra of $3Li_2O$-B_2O_3 target and as-deposited 3Li–B–O–N thin film.

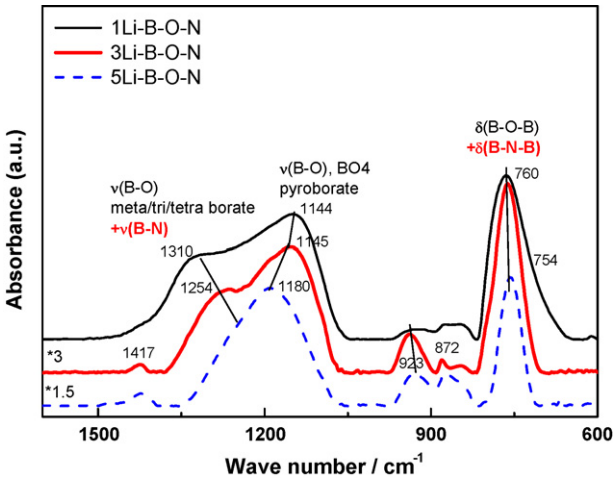

Fig. 4. FTIR spectral comparison of 1, 3 and 5Li–B–O–N thin films.

units. Other fingerprints in the low frequency region, which show the same trend of red shift, confirm that increase in lithium content together with N-doping results in complete destruction of ring-type structure.

The additional experimental clues for the N-doping to the films and the lithium content-dependent N-doping behavior were obtained from XPS analyses. Fig. 5 shows the N 1s spectra of the films. The presence of N 1s peak near 397.5 eV identifies that B–N bonds [11] exist in Li–B–O–N films. As increasing lithium content, the intensity of N 1s peak gradually decreases. Lithium content seems to play a control role in determining the doping level of N atom, consistent with elemental analyses results (Table 1). This is also correlated to the FTIR analyses results that as increasing lithium content, the LBO target with a boroxol ring structure tended to convert its structure to an open-type one of tetraborate/metaborate/etc. that possesses ionic characteristics, thereby, results in limited N-substitution. The substitution of N for some oxygen will reduce high polar bonding nature of oxygen, which in turn provides weaker polar bonding between B and N, resulting in enhanced mobility of lithium ions. In order to optimize the ionic conductivity of lithium ions, the appropriate amounts of Li_2O in xLi_2O–B_2O_3 and N-doping must be incorporated to the Li–B–O–N films.

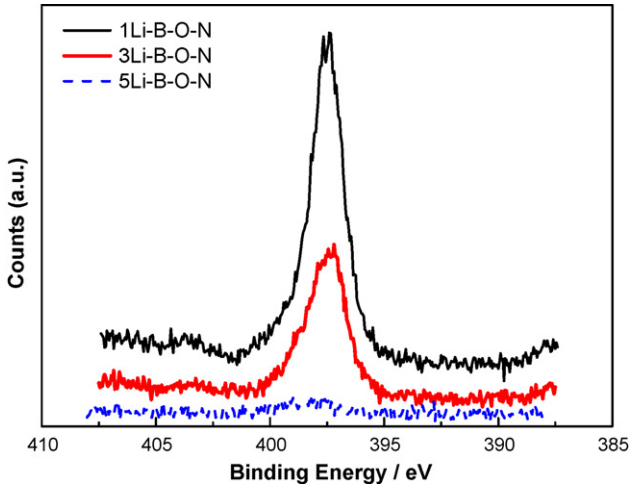

Fig. 5. N 1s XPS spectral comparison for 1, 3 and 5Li–B–O–N thin films.

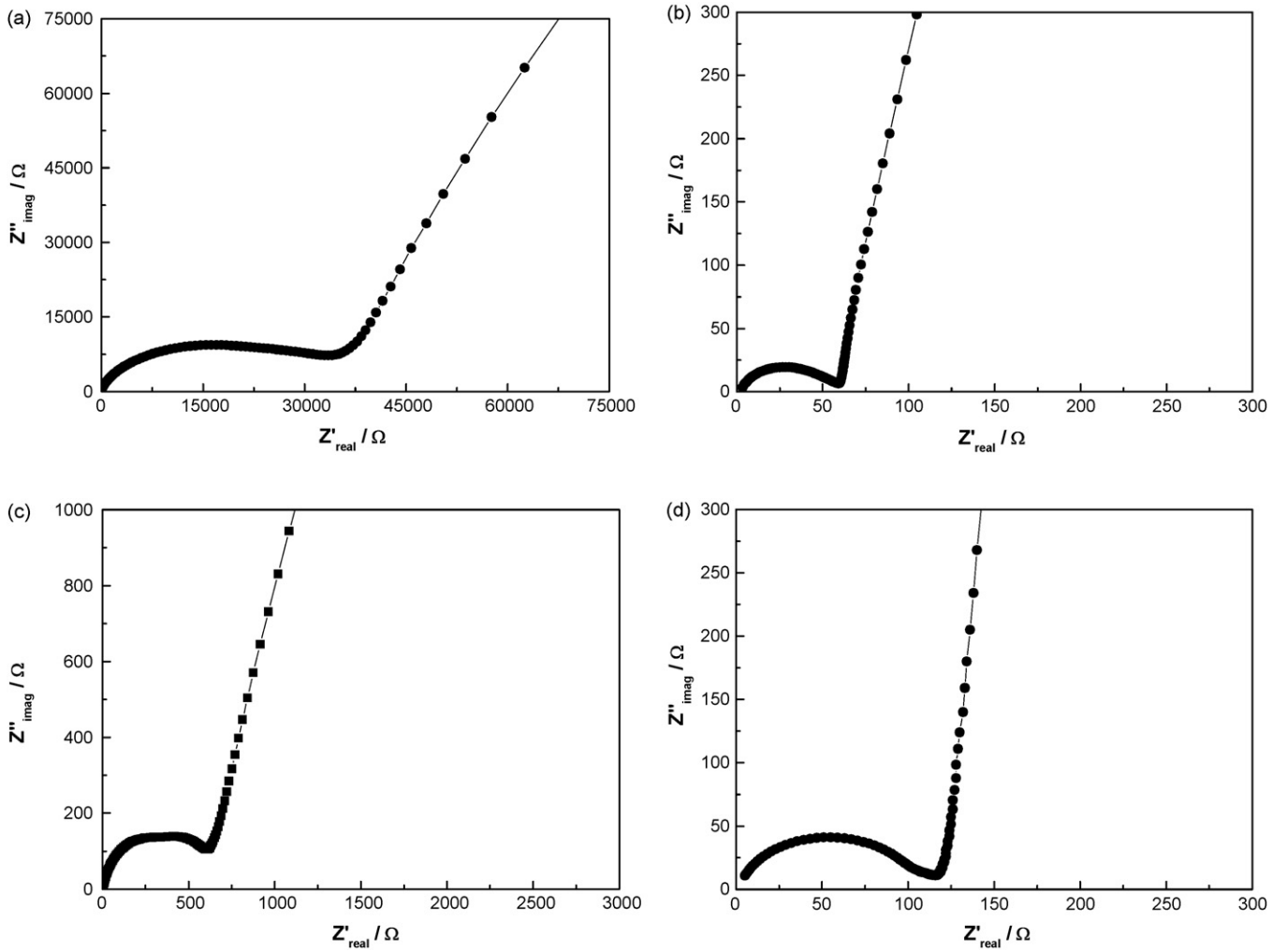

Fig. 6. Comparative electrochemical impedance spectra for blocking electrode cell at room temperature for (a) 1Li–B–O–N, (b) 3Li–B–O–N, (c) 5Li–B–O–N and (d) Lipon films.

3.2. Electrochemical properties of Li–B–O–N thin films

Fig. 6 shows impedance spectra for blocking electrodes cell of Pt/*x*Li–B–O–N/Pt with active electrode area of 1 cm^2. The resistances of electrolytes calculated from semi-circle of Nyquist plots increase as R(3Li–B–O–N) < R(5Li–B–O–N) < R(1Li–B–O–N). Table 2 summarizes the calculated ionic conductivity (σ) according to the following Eq. (1). The 3Li–B–O–N film exhibited the largest ionic conductivity of ca. 2.3×10^{-6} S cm^{-1} at room temperature, similar to or even larger than that of Lipon (1.2×10^{-6} S cm^{-1}) prepared in our group. This result suggests that we can achieve a lithium borate solid electrolyte with high ionic conductivity, which is enough for a use in thin film batteries at room temperature.

$$\sigma = \frac{(d/A)}{R} \tag{1}$$

Table 2
Ionic conductivities of Li–B–O–N and Lipon thin films obtained from impedance spectral analyses.

Targets	Thin films	Thickness (μm)	R (Ω)	σ_{25} (S cm^{-1})
1LBO	1Li–B–O–N	1.5	35,083	4.3×10^{-9}
3LBO	3Li–B–O–N	1.4	61	2.3×10^{-6}
5LBO	5Li–B–O–N	1.6	611	2.6×10^{-7}
Li_3PO_4	Lipon	1.5	120	1.2×10^{-6}

where d is thickness of solid electrolyte, A is electrode/electrolyte interface area, R is resistance from EIS.

Activation energy (E_a) for lithium ion conduction for 3Li–B–O–N was calculated by the following Eq. (2), using the Arrhenius relationship and measured conductivity at various temperatures (Fig. 7).

$$\sigma T = (\sigma T)_0 \exp\left(-\frac{E_a}{kT}\right) \tag{2}$$

where σ is lithium ionic conductivity, k is Boltzmann constant, T is temperature.

Activation energy of 3Li–B–O–N (0.49 eV) was smaller than that of Lipon (0.56 eV) reported in the previous work [12], indicating higher lithium ion mobility of 3Li–B–O–N than that of Lipon. Enhanced cycling performance at high rate or low temperature is expected.

Electrochemical stability and electrical conductivity that are essential criteria for solid electrolyte were evaluated by LSV for 3Li–B–O–N and Lipon with the same dimension (active area; 1×1 cm^2, thickness; 1.5 μm). In Fig. 8, for both electrolyte films, the current increase hardly occurred throughout the scanned potential range (0–5 V). However, Lipon film showed a slight current change above 3 V. This indicates that 3Li–B–O–N may have the slightly improved stability compared with Lipon and remains stable at high potential above 3 V, where lithium batteries are usually operated.

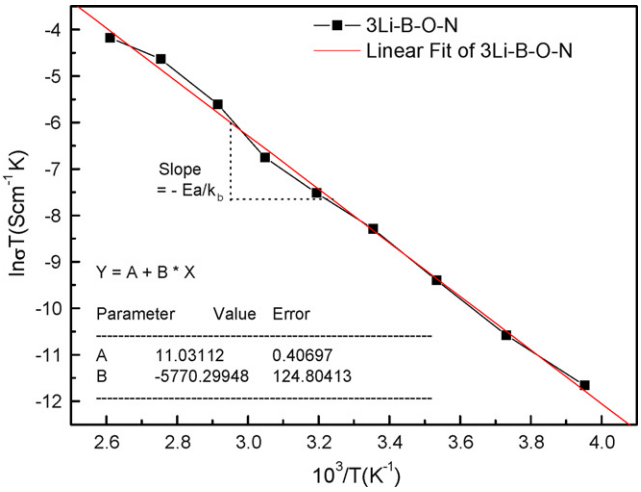

Fig. 7. Arrhenius plot for the ionic conductivity of 3Li–B–O–N film as a function of temperature.

The battery with 3Li–B–O–N electrolyte is therefore predicted to show lower self-discharge than Lipon.

Fig. 9 shows the discharge behavior of two identical thin film batteries composed of $LiCoO_2$ cathode and Li anode films, but different electrolyte films, 3Li–B–O–N and Lipon, respectively. Comparing the discharge capacities of these two batteries at room temperature, 3Li–B–O–N retained 98% of the initial capacity over 6 weeks while keeping at charged state of 4.1 V, whereas Lipon exhibited 93% of the initial capacity over the same period. The stability difference seems to be due to the fact that boron usually has

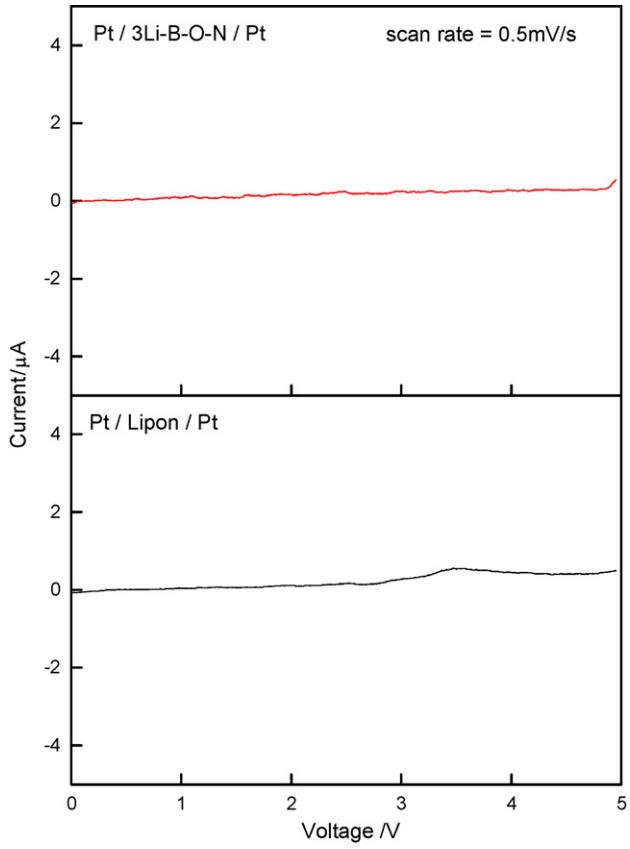

Fig. 8. Linear sweep voltammograms for blocking electrode cells with 3Li–B–O–N and Lipon films.

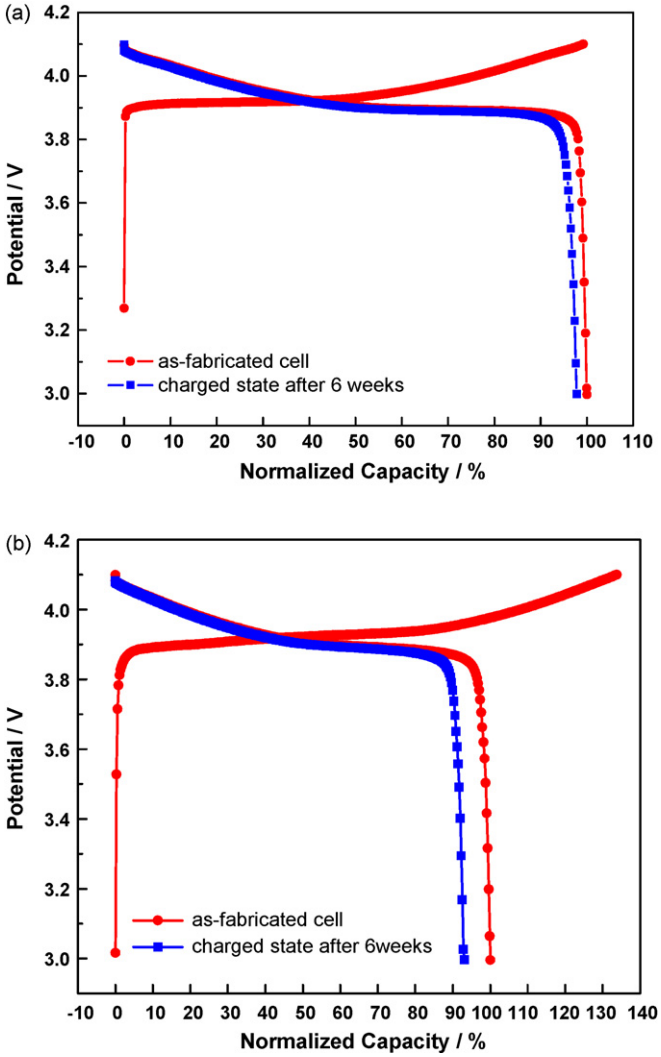

Fig. 9. Discharge profiles after 6 weeks aging of thin film batteries of $LiCoO_2$//Li system including (a) 3Li–B–O–N and (b) Lipon electrolyte, respectively.

the simple oxidation state of +3, while phosphorous probably possesses such multiple valences of −3, +1 and +5, thereby, electrical conductivity can change in non-homogeneous local region of Lipon during cycling [3]. The 3Li–B–O–N appears to be very stable in the operation potential range of thin film lithium batteries.

4. Conclusion

The *x*Li–B–O–N films were successfully obtained by reactive sputtering under pure nitrogen plasma using sputtering targets of xLi_2O–B_2O_3 (x = 1, 3, 5). The rocking chair concept with $LiCoO_2$/Li–B–O–N/Li multi-layer structure appears to function well in an all-solid-state rechargeable thin film battery. The maximum lithium ionic conductivity of ca. 2.3×10^{-6} S cm^{-1} at room temperature was obtained from $Li_{3.09}BO_{2.53}N_{0.52}$ thin film whose activation energy was 0.49 eV. By varying Li content and nitrogen-substitution level, the ionic conductivity of Li–B–O–N films could be controlled, thereby results in the activation energy for Li^+ ion conduction. Enhanced ionic conductivity appears to be due to the reduced strain energy by the creation of non-bridging oxygen in borate network and the reduced electrostatic energy by mixed anion effect. We propose Li–B–O–N thin film as a promising inorganic solid electrolyte for thin film lithium batteries.

Acknowledgement

This work was performed under the auspices by the Korea Energy Management Corporation under contact no. 2006-E-EL02-P-01.

References

[1] J.B. Bates, N.J. Dudney, G.R. Gruzalski, R.A. Zuhr, A. Choudhury, C.F. Luck, J.D. Robertson, J. Power Sources 43–44 (1993) 103.
[2] X. Yu, J.B. Bates, G.E. Jellison Jr., R.X. Hart, J. Electrochem. Soc. 144 (1997) 524.
[3] P. Birke, W.F. Chu, W. Weppner, Solid State Ionics 93 (1997) 1.
[4] P. Birke, W. Weppner, Electrochimica Acta 42 (1997) 3375.
[5] Y. ITO, K. Miyauchi, T. Oi, J. Non-cryst. Solids 57 (1983) 389.
[6] M. Eddrief, P. Dzwonkowski, C. Julien, M. Balkanski, Solid State Ionics 45 (1991) 77.
[7] S. Sakka, Annu. Rev. Mater. Sci. 16 (1986) 29.
[8] H.Y. Park, S.C. Nam, Y.C. Lim, K.G. Choi, K.C. Lee, G.B. Park, J.B. Kim, H. Park Kim, S.B. Cho, Electrochim. Acta 52 (2007) 2062.
[9] E.I. Kamitsos, G.D. Chryssikos, J. Mol. Struct. 247 (1991) 1.
[10] G. Socrates, Infrared Characteristic Group Frequencies; Tables and Charts, 2nd ed., John Wiley & Sons, 1994.
[11] X. Gouin, P. Grange, L. Bois, P. L'Haridon, Y. Laurent, J. Alloys Compd. 224 (1995) 22.
[12] US Patent #5,338,625.